Hydroxyapatite nanopowders obtained by sol-gel method, synthesis and properties

B. A. SAVA[a,*], C. TARDEI[b*], C. M. SIMONESCU[c], L. BOROICA[a], A. MELINESCU[c]
[a]*National Institute of Laser, Plasma and Radiation Physics, 409th Atomistilor str., 077125, Magurele, Romania,*
[b]*National Institute for R&D in Electrical Engineering ICPE-CA, 313 Splaiul Unirii, 031066, Bucharest, Romania,*
[c]*University Politehnica of Bucharest, Faculty of Applied Chemistry and Materials Science, 1 – 7 Polizu Str., 011061, Bucharest, Romania*

The present paper deals with sol-gel preparation of hydroxyapatite powders for bio uses by performing several techniques of gelation and thermal treatments of dried gels. The hydroxyapatite formation and decomposition are checked by X-ray diffraction which showed that the tri-calcium phosphate apparition takes place as the result of thermal treatment at 700^{o}C. The Fourier Transform Infrared spectra confirm the hydroxyapatite apparition and also the carbonyl disappearance at 900^{o}C, which is responsible for the grey color of the powdered sample. SEM pictures showed spherique particles with narrow distribution, in the range of 35-50 nm dimensions.

(Received September 20, 2015; accepted October 28, 2015)

Keywords: Hydroxyapatite, Nanopowders, Sol-gel, FTIR, XRD, SEM, DTA

1. Introduction

In last years many attempts have been focused on the preparation of synthetic hydroxyapatite (HA), which is quite similar to bone apatite and has excellent bone connectivity. Forming and sintering of apatite crystals at low temperatures were the main contributions of the sol-gel process in comparison with conventional synthesis methods for HA powder [1, 2]. Hydroxyapatite (HA) is used effectively as a material for bio implants that is like bone apatite and has good biocompatibility [3, 4].

A modified sol-gel process to synthesize in less than 16 hours nano crystalline hydroxyapatite (NHA) powder for biomedical applications using calcium nitrate tetra hydrate [$Ca(NO_3)_2x4H_2O$] and phosphorus pentoxide [P_2O_5] as precursors, is previously presented and discussed [1]. The results showed that there was an increase in the size of nanocrystals HA (NHA), ranging from 30 nm for the sample treated at 600 °C and up to 500 nm for the sample heat-treated at 1200 °C [1].

Fathi and Hanifi [2] describe the synthesis of particles nano-HA by sol-gel method. The nanocrystalline powder of hydroxyapatite (HA) was prepared using $Ca(NO_3)_2x4H_2O$ and P_2O_5 by a simple sol-gel approach. The presence of both crystalline and amorphous phase in the dried precursor gel was confirmed by the valuation technique. Single phase HA has been identified in the heat-treated powder, in the XRD diffraction patterns. SEM and TEM showed that the powder obtained after heat-treatment at 600 ° C was composed of HA agglomerated nanocrystalline particles (25-28 nm). Increasing the sintering temperature and time could cause decomposition of β – tri-calcium phosphate HA and lime. Prepared nanocrystalline HA is capable of improving contact reaction and stability to bone interface in medical applications [2].

Agrawal and co-authors [3] describes a synthesis technique of HA powder by sol-gel. The product was sintered twice, at two different temperatures, 400 ° C and 750 ° C, to improve its crystallinity. The sintered powder was characterized to investigate the contents of phase, the morphology, type of bonds and the thermal stability [3].

Hydroxyapatite HA, as powder, was prepared by Feng and co-authors [5] by using another version of preparation by sol-gel method, from phosphorus pentoxide (P_2O_5) and calcium nitrate tetrahydrated ($Ca(NO_3)_2x4H_2O$). It has been found that after sintering at temperatures between 600 and 900 °C, the phase of the dominant powder was: at 800 and 900 °C, HA with small amounts of calcium oxide and phosphate h-tri-calcium phosphate (h-TCP), and only the phase HA it was observed at 600 to 700 °C. Using this technique, were obtained HA powders of 10-15 nm [5].

A pure HA ceramic nano-sized crystals were prepared by other simple sol-gel method by Anuar and co-authors [6]. Production of particles of HA particles were made by varying the agitation rate between 100 and 500 rpm and the sintering temperature from 600 °C to 800 °C. HA prepared by sintering at 600 to 800 ^{O}C has low crystallinity and carbonated apatite structure. By further characterization, HA particles could be used as immobilizer or solid support for attachment of microorganisms in the fermentation process. The biomaterial possesses good mechanical properties and large superficial surface for micro-organisms absorption through electrostatic interaction mechanism. Primary particles of HA were obtained smaller at higher speeds of stirring and elevated sintering temperature. However, the

crystallinity and crystallite size of HA increased with increasing the sintering temperature of the particles [6].

Important properties such as low water solubility, high specific surface area, high thermal and chemical stability and high ionic exchange capacity suggested that HA can be an effective sorbent for heavy metals environmental depollution [7, 8].

This paper presents the preparation of HA powder for heavy metals extraction by a sol-gel method designed to optimize the previous descripted methods, by using different preparing steps suited by several appropriate thermal treatments. Structural and thermal characterization of the obtained materials was made in order to investigate their structure and properties modifications when process parameters are different and to choose the optimum ones.

2. Experimental part

Preparation of the samples of hydroxyapatite by sol-gel method

The selected method has the following advantages: a simple and rapid hydroxyapatite gel obtaining, low processing temperature and small amount of water entering in the process, which facilitates the drying process and reduces the losses by volatilization.

There were developed two sol-gel methods, leading to compounds further noted HAG 1 and HAG 2, differenced by gel maturation time, each of them divided on two different gelation paths, first variant coded a) at 60 degrees Celsius, the second coded b) at ambient temperature of 20^{o}C for longer time pursuing the influence of the working temperature/ gelling time on the kinetics of gelling and HA formation. The sample HAG 2 was reproduced using same procedure and coded HAG 3 in order to see the reproducibility of the experiment.

The raw materials were p.a. grade: • phosphorus oxide, P_2O_5; • Calcium nitrate tetrahydrate $Ca(NO_3)_2x4H_2O$; • Ethanol, C_2H_5OH.

I. The procedure for the first sample coded HAG1, has the following steps:

a) Preparing of solution 1, named solP:

- There were weighted 7.097 g P_2O_5 using an analytical balance in a 250 mL Berzelius vessel;
- There were added 100 mL of ethanol over phosphorus oxide;
- The solution was stirred 42 min until the complete dissolution was achieved with a magnetic stirrer at medium speed;

b) Solution 2 was prepared, named solC:

- ✓ There were added 100 mL of ethanol into a 250 mL Berzelius vessel;
- ✓ There were weighted 39.437 g of $Ca(NO_3)_2x4H_2O$ with the analytical balance and added in ethanol;
- ✓ The solution was stirred until complete dissolution for a minimum of 20 min (22 min) with a magnetic stirrer at medium speed;

c) The SolP was added dropwise into solC for 20 min;

d) The sol was mixed for 10 minutes with one magnetic stirrer at medium speed. The pH was maintained at 0.5-1;

e) The obtained clear, transparent sol was divided into two equal parts: HAG1a and HAG 1b;

f) HAG 1a was isothermally boiled at 60 °C in water bath for 60 min under continuous stirring, and then the slightly yellow gel obtained was kept for ageing 24 hours at ambient temperature;

g) HAG 1b was stirred for 5 hours with a magnetic stirrer, and the transparent gel, slightly opaque, less viscous than the obtained HAG 1a gel was kept for maturation 24 hours at ambient temperature;

h) Both HAG 1a and HAG 1b gel samples were maintained for drying at the temperature of 80 °C for 24 h. Samples expanded during the process of drying quicker the HAG 1a sample. This proves that large quantities of gases were produced in short time along the drying process, at lower temperature in the case of the sample HAG 1a.

i) The two samples were divided into four equal parts; one remaining as control, the others were calcined at 600, 800 and 900 °C for 2 hours, following the program presented in the case of the samples calcined at 600 °C in table 1.

Table 1. Calcination program

Hour [h]	Temperature [^{o}C]
0	20
1.5	120
2.0	120
3.0	250
3.5	250
4.5	400
5.0	400
6.5	600
8.5	600
	Free cooling

The other samples were thermal treated by similar procedure with heating speed of 150^{o}C/h over 600 ^{o}C and 2 hours maintaining at the respective temperature.

II. The procedure for the second sample coded HAG2, was the same in first a) to e) steps, with the only difference that in this case P_2O_5 was added in ethanol. The obtained HAG2a and HAG2b samples were kept for gel maturation 72 hours instead of 24 hours in the case of HAG1 samples. The drying and calcination were made in the same conditions as for the HAG1 samples. In this case also the expansion took place quicker for the sample HAG2a. One HAG2b sample was treated for 2 hours at 600^{o}C and other 2 hours at 900^{o}C, in order to see if the hydroxyapatite decomposition is influenced by such treatment. Samples coded s where thermally treated for prolonged time, 6 hours instead of 2, at selected temperature. Sample coded HAG3 was treated at 1200^{o}C, for 2 hours, to see if tri-calcium phosphate and calcium oxide recombine to form again hydroxyapatite.

The thermal analysis, comprising thermogravimetric analysis (TG), derivative thermogravimetric analysis (DTG) and differential thermal analysis (DTA) was

performed using the apparatus: STA 409PC (Netzsch – Germany) with next conditions:

- Temperature domain: 25°C-1000°C;
- Heating rate: 10 K/min;
- Alumina crucibles;
- Atmosphere: static air
- mass of the samples thermal analyzed are shown in Table 7.

Measurement uncertainty:

- Temperature: 1.29%;
- For % Δm: 3.60% of the value of % Δm.

All hydroxyapatite ceramic powders were characterized using FT-IR spectroscopy, X-ray diffraction (XRD), scanning electron microscopy (SEM) measurements. Phase composition and crystallinity of prepared HAP particles were determined by X-ray diffraction (XRD, Bruker D-8 Advance, Germany) with CuKα radiation, λ = 1.5406 Å, generated at 35 kV and 25 mA. Data were collected over 2θ range of 20–60° with a step size of 0.010° and a count time of 0.2s.

The presence of functional groups was analyzed by FTIR spectroscopy using a SHIMADZU 8400 Spectrometer in the 400-4000 cm^{-1} range. The morphological properties of surface and the internal structure characteristics were evaluated through scanning electron microscopy (SEM), using scanning electron microscope type FESEM-FIB Auriga (Carl Zeiss, Germany). For this kind of analysis, samples were subject to a special process of preparation by cleaning for 6 min in plasma arc in a Plasma Cleaner FISCHONE Device.

3. Results and discussion

Structural and properties investigation of hydroxyapatite samples produced by the sol-gel method

3.1. X-ray diffraction

X-ray diffraction patterns for samples HAG 1a, HAG 1b and HAG 2a, calcined at 600 and 700°C are shown in Fig. 1 a-f), and characteristics obtained from the diffractograms are presented in Table 2.

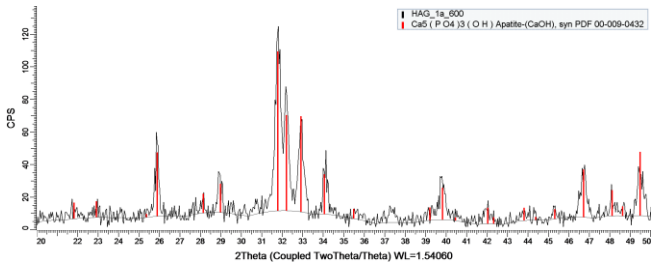

a)

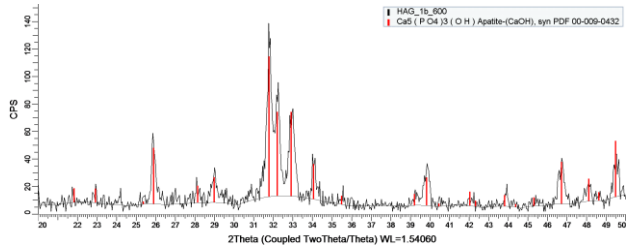

b)

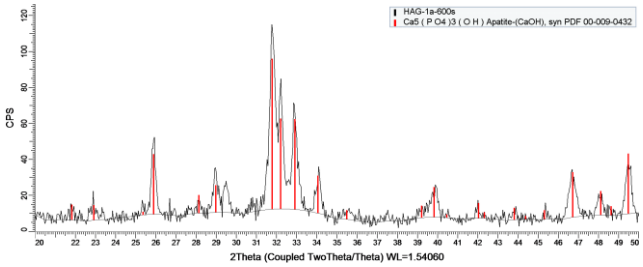

c)

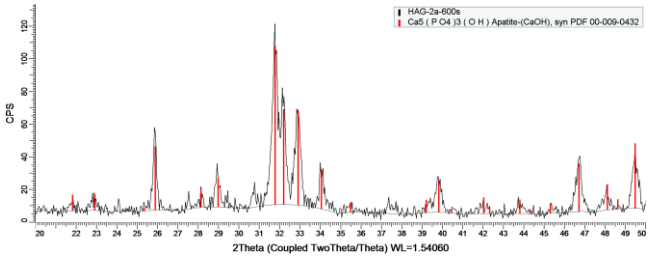

d)

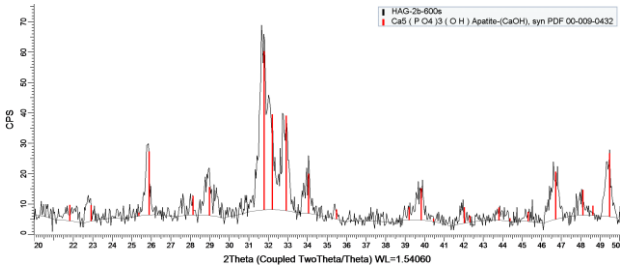

e)

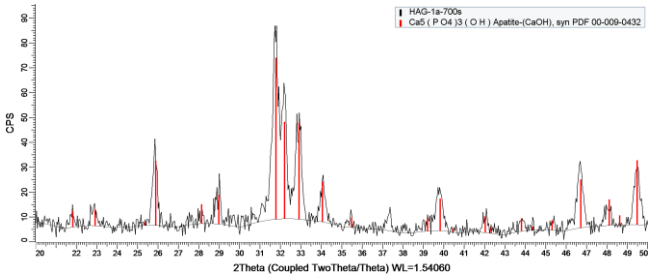

f)

Fig. 1. X-ray diffractogram of the samples: a) HAG 1a calcined at 600°C; b) HAG 1bcalcined at 600°C; c) HAG 1as calcined at 600°C; d) HAG 2a calcined at 600°C; e) HAG 2b calcined at 600°C and f) HAG 1a sample, calcined at 700°C

Table 2. Average particle size, fraction of crystalline phase and specific surface area for the samples HAG 1a, 2a and 1b, calcined at 600 and 700 °C, respectively obtained from the diffractograms

Sample	D[211] (nm)	Xc, [%]	S_{sp}, [m^2/g]
HAG_1a_600	58.45	0.65	32.48
HAG_1b_600	39.97	0.67	47.50
HAG_1a_600s	39.38	0.65	48.21
HAG_1a_700s	46.45	0.60	40.87
HAG_1b_700s	46.72	0.81	40.64
HAG_2a_600s	41.12	0.81	46.17
HAG_2b_600	36.86	0.54	51.51

The average particle size is calculated from XRD data using the Scherrer equation:

$$D = (k\lambda)/(\beta_D \cos\theta) \quad (1)$$

where D is the particle size in nanometer, as calculated for the [211] reflection, λ is the wavelength of CuKα1 radiation (1.5406 Å), β_D is the full width at half maximum for the diffraction peak under consideration, θ is the diffraction angle and k is the broadening constant, which is close to unity.

The fraction of the crystalline phase of hydroxyapatite in the samples X_c was calculated using the formula:

$$X_c = 1 - \frac{V_{112/300}}{I_{300}} \quad (2)$$

where Xc is the fraction of crystalline phase, I_{300} is the intensity of (300) diffraction peak and $V_{112/300}$ is the intensity of the trough between (112) and (300) diffraction peaks.

The specific surface area was calculated with the formula:

$$S_{sp} = 6 \times 10^3 / d \times \rho_{th} \quad (3)$$

where d is the average particle diameter and the theoretical density of the hydroxyapatite is ρ_{th} (HAP) = 3.16 g/cm^3 for spherical particles.

The XRD patterns of samples HAG 1a, HAG 1b, HAG 2a and HAG 2b calcined at 600 °C indicated only the presence of the hydroxyapatite. In the case of the sample HAG 1a, calcined at 700°C it appears a maximum specific to tri-calcium phosphate and a weak peak of calcium oxide (CaO) appeared in the pattern, which shows that at this temperature begins the decomposition of hydroxyapatite.

The proportion of crystalline phase of hydroxyapatite is between 0.65 and 0.81, higher for the sample HAG 2a and HAG 1b, treated for 6 h at 600 and 700°C respectively. The specific area was between 32.48 and 48.21 m^2/g and decreases with increasing thermal treatment temperature.

The b variant of gelation and shorter thermal treatment times leads to higher surface area. The sol-gel method 2 determines higher surface area comparatively to 1. In this case the gelation at room temperature (variant b) also leads to higher surface area.

X-ray diffraction patterns for samples HAG 2a, HAG 1b and HAG2b, calcined at 800°C are presented in Fig. 2 a-c), and characteristics obtained from the diffractograms in Table 3.

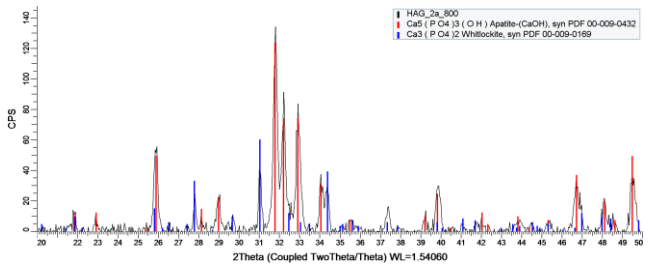

a)

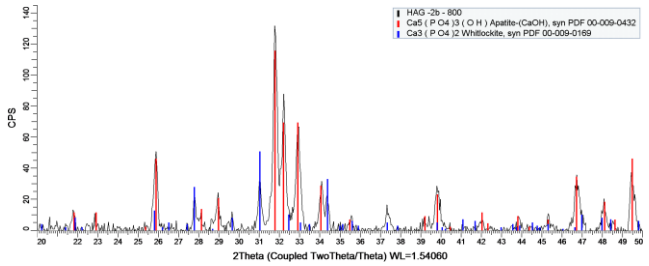

b)

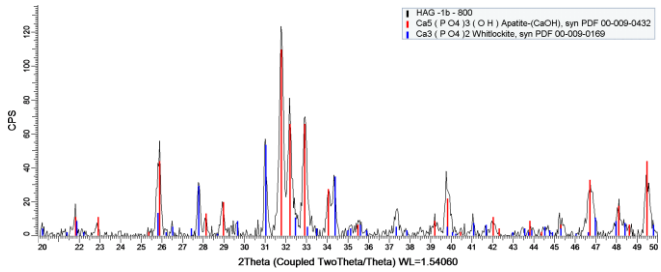

c)

Fig. 2. X-ray diffractogram of the samples: a) HAG 2a calcined at 800°C; b) HAG 2b sample, calcined at 800°C and c) HAG 1b sample, calcined at 800°C

Table 3. Average particle size, fraction of crystalline phase and specific surface area for the samples HAG 2a, HAG1b and HAG2b, obtained from the diffractograms for the samples calcined at 800°C

Sample	D[211] (nm)	Xc, [%]	S_{sp}, [m^2/g]
HAG -2a - 800	49.32	0.77	38.5
HAG -1b - 800	46.24	0.82	41.06
HAG -2b - 800	47.53	0.76	39.95

The XRD patterns of samples HAG 2a, HAG 1b and HAG 2b calcined at 800°C indicated the presence of hydroxyapatite and tri-calcium phosphate, which shows that at this temperature the heat treatment part of hydroxyapatite is decomposed. The proportion of crystalline hydroxyapatite phase is between 0.76 and 0.82, higher for sample 1b. The surface area is between 38.5 and 41.06 m^2/g, higher for sample 1b, proofing that the sample with gelation at room temperature and longer time is more suitable for heavy metals removal. X-ray diffraction patterns for samples HAG 1b, HAG 2a and HAG 2b, calcined at 900°C, are shown in Fig. 3 a-c) and the calculated characteristics from diffractograms in Table 4.

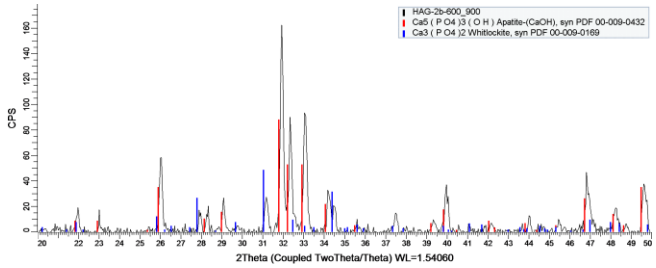

a)

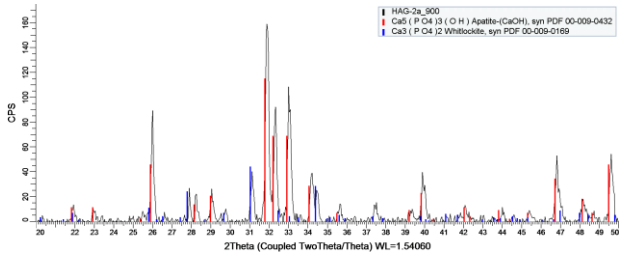

b)

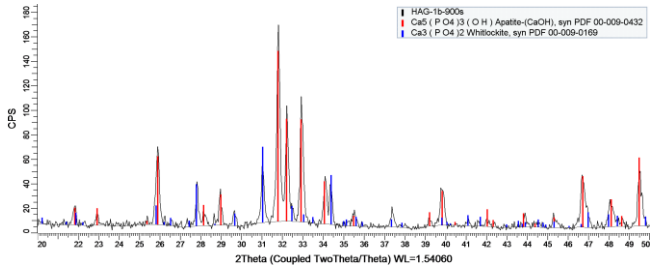

c)

Fig. 3. X-ray diffractogram of the samples: a) HAG 2b calcined at 600 and 900°C; b) HAG 2a calcined at 900°C; c) HAG 1bs, sample, calcined at 900°C

Table 4. Average particle size, fraction of crystalline phase and specific surface area for the samples HAG 2a, 1b and 2b, obtained from the diffractograms for the samples calcined at 900°C

Sample	D[211] (nm)	Xc, [%]	S_{sp}, [m^2/g]
HAG_2b_600_900	55.90	0.94	33.97
HAG_2a_900	50.17	0.96	37.85
HAG_1b_900	55.13	0.90	34.44

The XRD patterns of samples HAG 2a, HAG 1b and HAG 2b calcined at 900°C indicated the presence of hydroxyapatite and tri-calcium phosphate, which showed that at this temperature the heat treatment an important part of hydroxyapatite is decomposed. It can also be seen that additional crystalline phases (β-TCP and CaO) appear at 800 and 900°C. It could be concluded that HA could be decomposed into β-TCP and CaO as the sintering temperature is at 750°C or above.

The crystallite size is close for the two methods of gelation and increases with increasing heat treatment temperature. The proportion of crystalline phase is between 0.54 and 0.96, higher for the sample HAG 2a. The specific surface area is between 34.44 and 51.51 m^2/g and decreases with increasing heat treatment temperature.

It can be concluded from the data provided that the decomposition of the hydroxyapatite to form calcium phosphate weakly begins in samples treated at 700°C and is already important in samples annealed at 800°C and especially for those treated at 900°C. The proportion of the crystalline phase is higher in the case of the samples gelled at room temperature, for both HAG1 and HAG 2 samples and the specific surface area, as expected, decreases with increasing heat treatment temperature.

The calcination at higher temperature in the case of the HAG3 sample, which presented the same characteristics as sample HAG2 leads to the recombining of tri-calcium phosphate and calcium oxide to form hydroxyapatite again as presented in Fig. 4 similar to Figueroa and coauthors results [1].

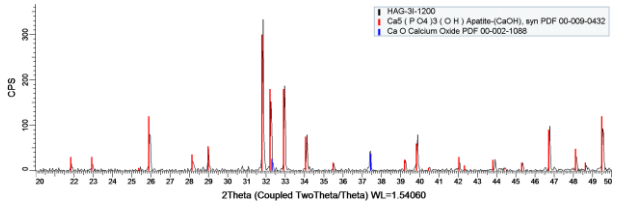

Fig. 4. X-ray diffraction pattern of HAG3 sample, calcined at 1200°C

3.2. FTIR spectroscopy

FTIR spectrograms for samples HAG 2a- dry, HAG 2b - dry, HAG 1 - heat treated at 600°C, HAG 1b - heat treated at 600°C, HAG 2b - heat treated at 600°C, HAG 2a - heat treated at 900°C, HAG 1b - heat-treated at 900°C and HAG 2b heat-treated at 600°C and 900°C are shown in Fig. 5-7.

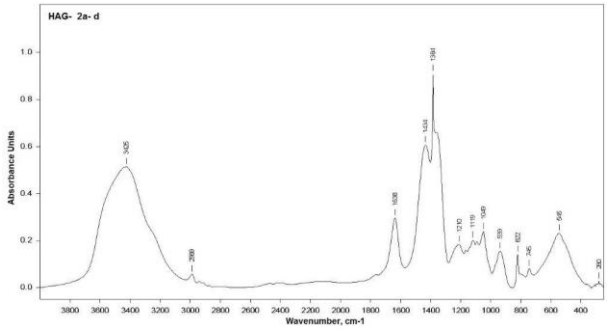

a)

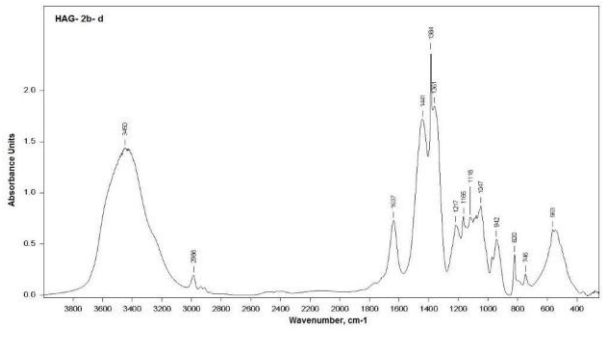

b)

Fig. 5. FTIR absorption spectra for the samples: a) HAG 2a dry; b) HAG 2b dry

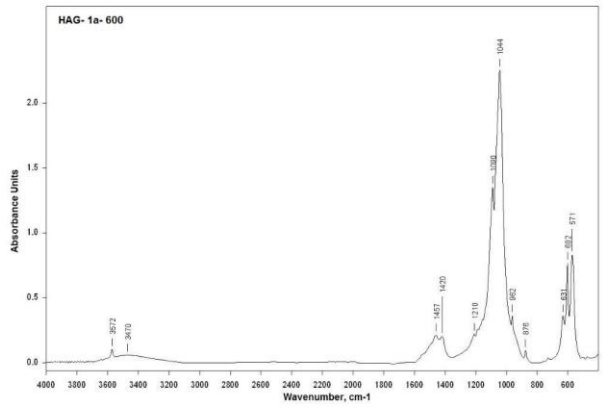

a)

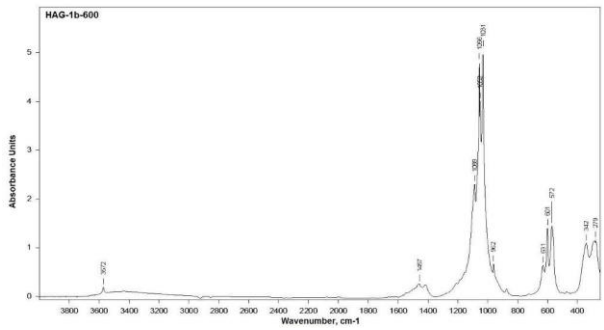

b)

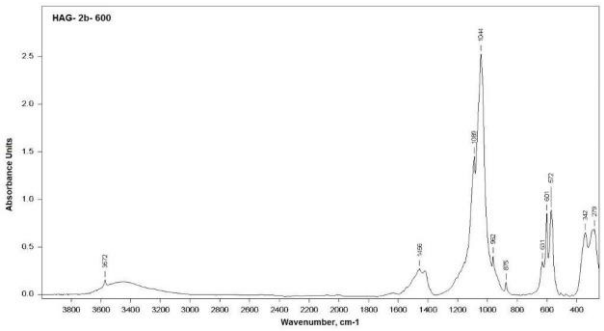

c)

Fig. 6. FTIR absorption spectra for the samples a) HAG 1a heat-treated at 600^{o}C; b) HAG 1b heat-treated at 600^{o}C; c) HAG 2b heat-treated at 600^{o}C

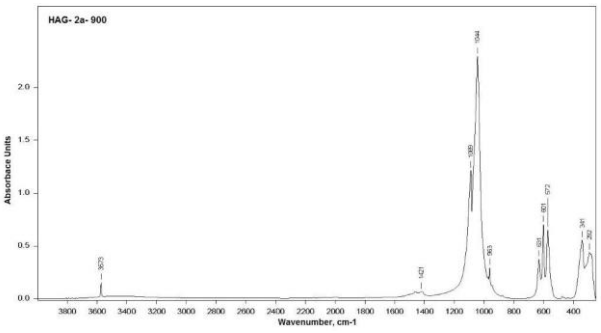

a)

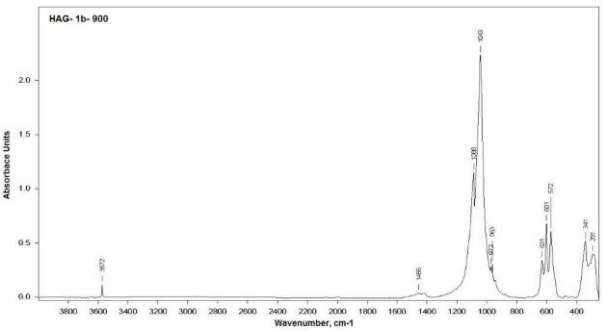

b)

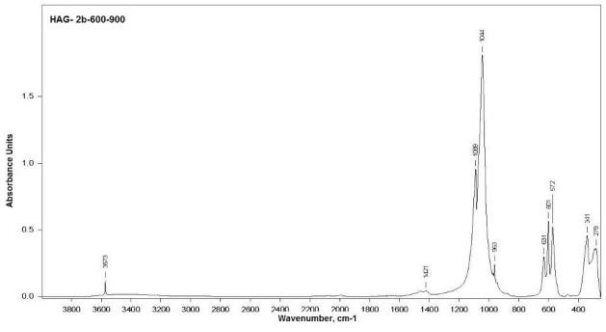

c)

Fig. 7. FTIR absorption spectra for the samples: a) HAG 2a heat-treated at 900^{o}C; b) HAG 1b heat-treated at 900^{o}C; c) HAG 2b heat-treated at 600 and 900^{o}C

Table 5 shows the FTIR absorption peaks and their assignation, according to literature.

Table 5. FTIR absorption maxima and their attribution

Sample code FTIR maximum [cm^{-1}] Assignation	HAG 2a dry	HAG 2b dry	HAG 1a 600° C	HAG 1b 600° C	HAG 2b 600° C	HAG 2a 900°C	HAG 1b 900°C	HAG 2b 600°C-900°C
	280	-	-	279	279	292	291	279
	-	-	-	342	342	341	341	341
Asymmetrically bending PO_4^{3-} [3]	545	563	571	572	572	572	572	572
Bending PO_4^{3-} [6]	-	-	602	601	601	601	601	601
Asymmetrically bending PO_4^{3-} [3]	-	-	631	631	631	631	631	631
Surface hydroxyl group (OH^-)[6]	745	745	-	-	-	-	-	-
Surface hydroxyl group (OH^-)[6]	822	820	-	-	-	-	-	-
(CO_3^{2-}) type B substituted [6]	-	-	876	-	875	-	-	-
Symmetrically stretching PO_4^{3-} [3]	939	942	962	962	962	963	963	963
Asymmetrically stretching PO_4^{3-} [6]	1049	1047	1044	1031	1044	1044	1043	1044
Asymmetrically stretching PO_4^{3-} [6]	1119	1118	1090	1089	1089	1089	1088	1089
	-	1165	-	-	-	-	-	
	1210	1217	1210	-	-	-	-	-
(CO_3^{2-}) type A substituted [6]	-	1361	-	-	-	-	-	
(CO_3^{2-}) type A substituted [6]	1384	1384	-	-	-	-	-	-
(CO_3^{2-}) type A substituted [6]	1434	1441	1420	1420	1421	1421	1425	1421
(CO_3^{2-}) type A substituted [6]	-	-	1457	1457	1456	-	-	
Water (H_2O)	1638	1637	-	-	-	-	-	
Water (H_2O)	2989	2986	-	-	-	-	-	-
Water (H_2O)	3425	3450	3470	-	-	-	-	-
Stretching O-H [3, 6]	-		3572	3572	3572	3573	3572	3573

The bands of adsorbed water (H_2O) which appear in 1600-3500 cm^{-1} domain for the dry samples – Fig. 5, Table 5, are much lower in the case of samples treated at 600 and almost disappear at samples burned at 900°C – Figs 6-7, Table 5, are due to the hygroscopic character of the crystalline carbonated HA. Bands assigned to OH group appear in dry samples at 745 and 820-822 cm^{-1} – Table 5, assigned to small parts of pyrophosphate either from the raw materials or appeared in course of sol-gel reactions. It was mentioned that bands at 732.8 cm^{-1} corresponding to the OH group appeared in calcium phosphates containing phases with calcium pyrophosphate in the sample [6].

The positions and dimension of the peaks of (CO_3^{2-}) group indicate the minor formation of B-type and A-type carbonated HA [6]. Initially at lower sintering temperature these peaks are broad but with increase of sintering temperature the peaks get ill-defined due to elimination of (CO_3^{2-}) [3]. Bands allocated to carbonated groups (CO_3^{2-}) [6] at 875-876 and 1420-1457cm^{-1} appeared in the samples calcined at 600°C but for those calcined at 900°C almost disappear (this is the explanation of the gray color of samples burned at 600 and 700^{o}C, which disappears for samples fired at 900^{o}C). It is known that the hydroxyl and the phosphate sites in the HA lattice can be substituted by carbonate ions that resulting in type A or type B apatite [6]. The presence of carbonate ions in apatite structure is believed to be taken place during the HA preparation whereby the atmospheric CO_2 can react with hydroxyl ions forming carbonate ions [6].

The absorption band at 3572-3573 cm^{-1}, attributed to the stretching of O-H bond confirms the presence of hydroxyapatite in all the samples heat treated at 600 and 900°C – figs 6-7, Table 5. Authors assigned the sharp peaks 3570 cm^{-1} and 3670 cm^{-1} to the stretching vibration of the lattice OH^- ions [3]. The OH- stretching vibration is unique for crystalline hydroxyapatite and its intensity is considerably weaker for all the samples, compared to the strong P-O stretching vibration, because of the hydroxyapatite stoichiometry. Both HAG1 and HAG2 thermal treated samples present characteristic peaks for PO_4^{3-} groups at 962-963 and 631cm^{-1}. Strong asymmetric stretching bands of phosphate ion from 1037-1049 and 1088-1129 cm^{-1} also confirm the formation of hydroxyapatite [6].

3.3. Thermal Analysis TG / DTA + DTG

Two dried samples was thermal analysed with mass indicated in Table 6.

Table 6. Mass of the samples thermal analyzed

Sample	Mass of analyzed samplee/mg
HAG-2a (dry)	28.79
HAG-2b (dry)	28,87

The thermograms of the analyzed samples are shown in Figs. 8-9.

Tables 7 and 8 show detailed results of the TG, DTG, DTA analysis for the dried HAG 2a and HAG 2b samples. In both cases there appears two endothermic effects at low temperature (with heating peaks around 60 and 120°C respectively) and one at higher temperature (720-740°C), between whom two exothermic picks are evidenced, at 260-290^{o}C and at 415-445^{o}C. The first two endothermic peaks, at low temperature are due to evaporation of ethanol, respectively water, the third one at high temperature is due to the decomposition of the hydroxyapatite forming tri-calcium phosphate. The first exothermic peak from 260-290°C is due to the formation of hydroxyapatite [3]. The second one is due to the decomposition of unreacted calcium nitrate, with the formation of hydroxyapatite [3].

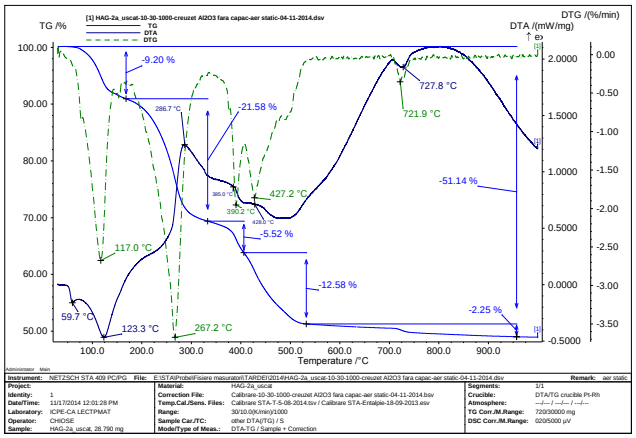

Fig. 8. TG, DTG and DTA curves for sample HAG-2a (dry)

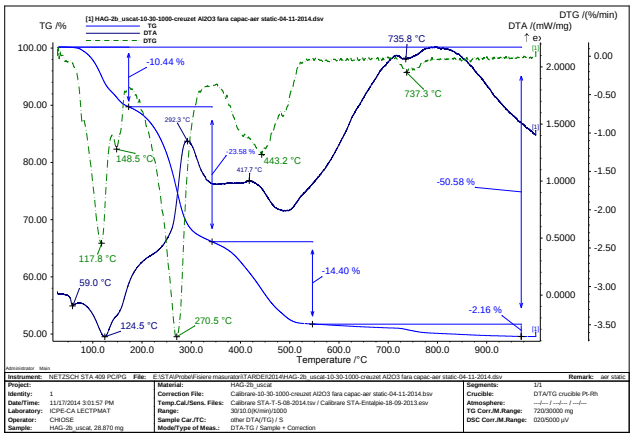

Fig. 9. TG, DTG and DTA curves for sample HAG-2b (dry)

As it can be seen from Figs. 8-9 and table 7 and 8, the temperature domains for endothermic and exothermic peaks are close in both cases, slightly higher in the case of exothermic reactions for sample 2b, which indicates higher stability of the gel. The decomposition of the formed hydroxyapatite takes place at higher temperature in the second case, meaning that hydroxyapatite is more stable in this case, which was confirmed by the XRD data.

In the case of 2b sample the decomposition of unreacted raw materials is pointed out by only one second exothermic peak, comparatively to 2a sample, which presents two exothermic peaks in the 390-420 ^{o}C temperature domain. The mass loss is lower in this temperature domain in the case of 2b sample, which proves that the gel formation at room temperature is the best because the formed and matured gel is more stable in this case and also the formed hydroxyapatite has higher decomposition temperature, as shown before.

Table 7. Characteristic parameters of non-isothermal degradation of the sample HAG-2a (dry)

Process	ΔT /(°C)	%Δm/%	T_{min}(DTG)/ (°C)	Pick DTA/(°C)	ΔH	$\%\Delta m_{total}$/%
1	25-75	-	-	59,7	endo	51,13
2	75-175	9,20	117,0	123,3	endo	
3	175-335	21,58	267,2	286,7	exo	
4	335-415	5,52	390,2	385,0	exo	
5	415-535	12,58	427,2	428,0	exo	
6	535-960	2,25	721,9	727,8	endo	

ΔT = the temperature domain in that occurred the process; %Δm = mass loss in process; $\%\Delta m_{total}$ = Total Mass Loss; T_{min}(DTG) = minimum appropriate temperature DTG; pick DTA = proper temperature minimum / maximum DTA; ΔH = endothermic effect (endo) / exothermic (exo) [9]

Table 8. Characteristic parameters of non-isothermal degradation of the sample HAG-2b (dry)

Process	ΔT /(°C)	%Δm/%	T_{min}(DTG)/ (°C)	Pick DTA/(°C)	ΔH	$\%\Delta m_{total}$/%
1	25-75	-	-	59	endo	50,58
2	75-175	10,44	117,8; 148,5	124,5	endo	
3	175-345	23,58	270,5	292,3	exo	
4	345-545	14,4	443,2	417,7	exo	
5	545-970	2,16	737,3	735,8	endo	

3.4. SEM investigations

The HAG-2a and 2b samples, treated at 800°C were investigated using SEM. The obtained photos, at 100 K magnification, are presented in Fig. 10 a - b).

The SEM photos for HAG2a and HAG2b powders shows that the structural units of obtained HA powders are relatively homogeneous in size and have spherical shape. Nanometer microstructures with crystallite dimensions in the range of 35-50 nm are evidenced. HAG a samples are compact, well densified and present macroporosity (250-400nm) sporadic and not interconnected.

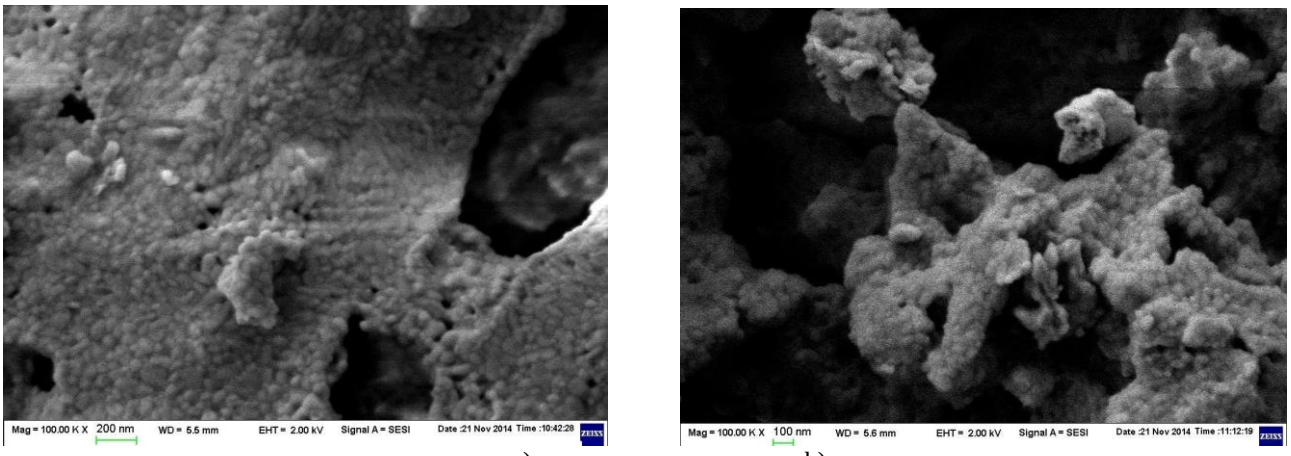

a) b)

Fig. 10. SEM photos of HAG-2a – a) and HAG-2b - b) samples, thermally treated at 800°C

The materials are strong agglomerated as consequence of high reactivity of small and homogeneous distributed particles.

4. Conclusions

The sol-gel method used for HAG1-3 samples obtaining has several advantages over other techniques comprising simplicity and shorter gelation time together with no necessary pH control and short hydrolysis time.

The sol-gel obtained HA powders which were treated under 700°C contains only hydroxyapatite as proved by XRD. For the ones treated at 700°C tri-calcium phosphate and calcium oxide begin to form by hydroxyapatite decomposition, evidenced by specific XRD peaks apparition. When the temperature of thermal treatment is 800°C and especially at 900°C a more important part of

hydroxyapatite is decomposed, as revealed by XRD patterns. XRD pattern for the sample calcined at 1200^{o}C shows that tri-calcium phosphate and calcium oxide recombine forming hydroxyapatite again.

The crystalline phase proportion lies between 0.54 and 0.96 for sol-gel samples thermally treated in 600-800^{o}C domain. The specific surface area is between 34.44 and 51.51 m^2/g and decreases as thermal treatment temperature increases.

SEM and XRD calculations revealed that primary HA particles of nanometer size were produced for high sol stirring speed and xero-gels sintering temperature. The dimension and crystallinity of crystallites increased as sintering temperature increased, due to particles increasing and agglomerating.

Acknowledgements

The research was financed by the Ministry of National Education–Executive Unit for Financing Higher Education, Research and Development and Innovation (MEN–UEFISCDI) in the PARTNERSHIP in the priority areas PNII, program through project PARTNERSHIP 92/01.07.2014. (**PN-II-PT-PCCA, Contract No. 92/2014)** and **M-ERA.NET 7-081/2013 MAGPHOGLAS** project.

References

[1] I. A. Figueroa, O. Novelo-Peralta, C. Flores-Morales, R. González-Tenorio, M. C. Piña-Barba, Biomatter **2**(2), 71 (2012).
[2] M. H. Fathi, A. Hanifi, Materials Letters **61,** 3978 (2007).
[3] K. Agrawal, G. Singh, D. Puri, S. Prakash, Journal of Minerals & Materials Characterization & Engineering, **10**(8), 727 (2011).
[4] Ch. Ţârdei, L. Moldovan, O. Craciunescu, Romanian Journal of Materials, **1**, 41 (2010).
[5] W. Feng, L. Mu-Sen, L. Yu-Peng, Q. Yong-Xin, Materials Letters **59**, 916 (2005).
[6] A. Anuar, M. Nabil, A. Salimi, M. Zulkali, M. Daud, Y. F. Yee, Advances in Environmental Biology, Special Issue for International Conference of Advanced Materials Engineering and Technology (ICAMET 2013), Bandung, Indonesia, 2013, p. 3587.
[7] C. M. Simonescu, A. Tatarus, C. Tardei, D. Patroi, M. Dragne, D.C. Culita, Rev. Chim., **66** (5), 732 (2015).
[8] A. Melinescu, C. Tardei, C. M. Simonescu, V. Marinescu, A. Miclea, Romanian Journal of Materials, **43**(2), 223 (2013).
[9] C. Constantinescu, A. Rotaru, A. Nedelcea, M. Dinescu, Materials Science in Semiconductor Processing, **30**, 242 (2015).

*Corresponding author: christu.tardei@icpe-ca.ro
savabogdanalexandru@yahoo.com